International Journal of Applied Energy Systems, Vol. 4, No. 2, July 2022

High-Frequency Isolated Three-phase Grid-Tied PV Converter Based a New Boost Inverter Topology

Hamdy Radwan
faculty of Energy Engineering,
Aswan University,
Aswan, Egypt
hamdy_radwan@aswu.edu.eg

Mahmoud A. Sayed
Dept. of Electrical and Mechanical Engineering,
Nagoya Institute of Technology,
Nagoya - Japan
mahmoud_sayed@ieee.org

Takaharu Takeshita
Dept. of Electrical and Mechanical Engineering, Nagoya Institute of Technology,
Nagoya - Japan
take@nitech.ac.jp

Adel A. Elbaset
Department of Electrical Engineering,
Minia University,
El-Minia, Egypt
adel.Soliman@mu.edu.eg

G. Shabib
faculty of Energy Engineering,
Aswan University,
Aswan, Egypt
gabershabib@gmail.com

Abstract— This paper proposes a new topology of grid-tied PV applications. The full system consists of two-stages, high-frequency boost inverter cascaded by rectifier–inverter system. In the first stage, a new single-stage high-frequency boost inverter is designed to boost and convert the DC output voltage of the PV array to a high-frequency single-phase square waveform in addition to realizing maximum power point tracking (MPPT). The proposed topology enables high-frequency transformer to be used for providing galvanic isolation between the two-stages. The second stage is rectifier-inverter system that links the first stage to three-phase grid connected. Many advantages of the 5kW three phase grid connected proposed system are provided such as boosting the inverter output voltage level, MPPT, galvanic isolation, high reliability, small size, and light weight. In addition, a grid side controller is used to inject a sinusoidal current into the grid at unity power factor. The proposed topology has been verified analytically by using PSIM software.

Keywords— ***Converter control, Grid connected, High frequency power converter, High frequency transformer, Photovoltaic***;

I. Introduction

Newly, energy demand has increased expressively. Conventional energy sources such as fossil fuels are no longer adequate to cover energy demand especially in future that because they are non-renewable energy sources. Additionally, the carbon emissions of the conventional resources cause global warming. Consequently, the Need of renewable energy sources has enlarged to meet the energy demand beside the conventional sources [1-٣]. Furthermore, renewable energy has received excessive interest due to its obtainability, maintainability, safety, clean and dependability [٤].

Photovoltaic (PV) energy is one of the promising sources of renewable energy. Hence, the research is motivated in this direction to increase the reliability of PV energy resources. PV grid-connected system should accomplish some functions such as extracting the maximum power point tracking (MPPT), boosting the array voltage, providing galvanic isolation for safety purposes, injecting of high quality low harmonics AC power to the grid with unity power factor, and using high efficient operation [5-8].

Several topologies for PV grid connected inverter have been displayed; in general, grid-connected PV systems can be categorized into two topologies. One of them is with galvanic isolation, and anther is without galvanic isolation. The implementation of galvanic isolation can be achieved by using a line frequency transformer (LFT) or a high frequency transformer (HFT). Conversely, topologies without galvanic isolation are transformerless topologies.

Transformerless topologies [9-13] are more efficient, lighter, less expensive and less impression than the galvanic isolated topologies. On the other hand, the main problem that must be overcome in non-isolated PV inverters is the leakage ground currents through the PV module parasitic capacitance, furthermore to DC current injected to the grid [14]. Serious leakage current enhances system losses, decreases the quality of grid-connected current, prompts serious conducted and radiated electromagnetic interface and leads to personal safety issues. In order to keep the leakage and DC currents injected to the grid under control, complex solutions are needed.

It is known that the output voltage of the PV module is low compared to the grid voltage so voltage boosting procedure is required for grid connection. Consequently, LFT is extensively used [15-16]. Besides voltage boosting, LFT provides galvanic isolation between the PV system and grid that plays an essential role in safety purpose and protection. Accordingly avoiding DC current injection into the grid and eliminating leakage current. In spite of that, LFTs are heavy, large, and expensive, the entire system is bulky and difficult to install due to its low frequency [17-18]. Consequently, the topology LFT is considered as a poor solution, which is better to be replaced by HFT.

The use of HFT [19-22] ensures galvanic isolation between the utility grid and the PV system, as well as overcoming the disadvantages of using conventional LFT [23-24]. However, there is a scarcity of scientific research to use HFT with PV systems in a way that performs all the required functions, particularly MPPT.

This paper presents a new topology for interfacing PV array with the utility grid. The system consists of two stages. The first one is high-frequency boost inverter (HFBI), which gives a 10-kHz square wave output voltage to meet the requirements of HFT and configure a multi-featured system. The second stage is rectifier-inverter system (RIS), which injects a sinusoidal current with minimum harmonic distortion and unity power factor to the grid. This paper is arranged as follows; first, the schematic circuit of the proposed system is described. Second, the operating modes of the proposed topology are exhibited. Third, control methodologies are examined. Finally, simulations consider the fundamental operation waveforms of the proposed system.

ISSN: 2636 - 3712 (Printed Version)
ISSN: 2636 - 3720 (Online Version)

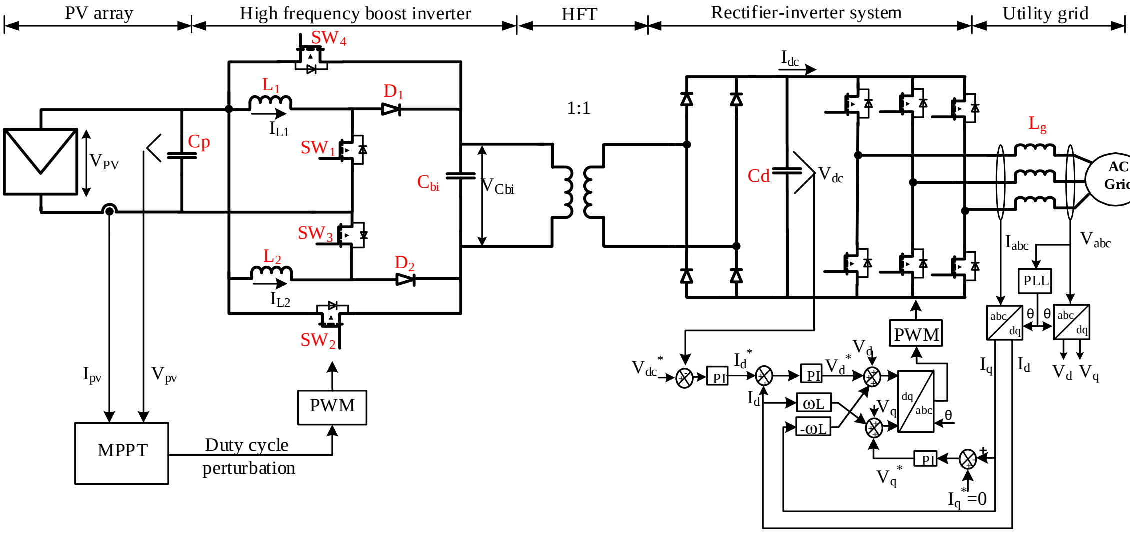

Fig.1. The proposed system

II. PROPOSED SYSTEM

A. Proposed topology (basic version)

The proposed system consists of two stages, High-frequency boost inverter (HFBI) cascaded by rectifier-inverter system (RIS) as shown in Fig. 1. Furthermore, the implemented switching control strategies are shown in the figure. The first stage is a redesign of the topology given in [7] to acquire a 10-kHz square wave output voltage rather than the fundamental grid voltage. HFBI consists of two buck-boost converters connected, as shown in Fig. 2. The second stage is simply approximated by a resistor. Each one of these converters operates sequentially in DCM for one half cycle of the targeted 10 kHz square waveform. DCM operation prevents the circulating currents between the inductor and the parallel-connected switch in the next operating half cycle. The power MOSFETS SW_1 and SW_3 are switched at high-frequency of 100 kHz while SW_2 (or SW_4) is kept continuously ON during the positive half cycle (or negative half cycle) of the targeted 10 kHz square waveform. Switches SW_1 and SW_2 operate to provide the positive boosted half-cycle, whereas SW_3 and SW_4 operate to provide the negative boosted half-cycle.

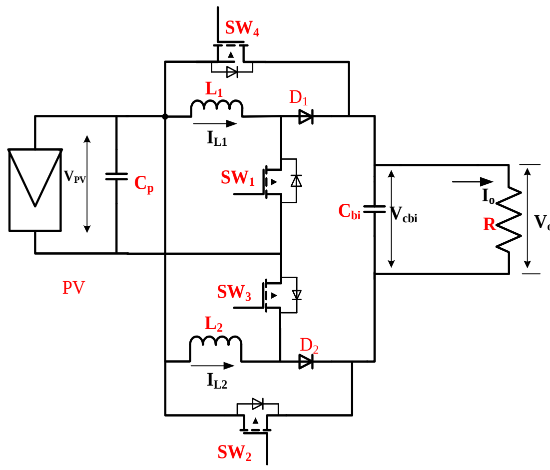

Fig. 2. Configuration of the single-stage HFBI

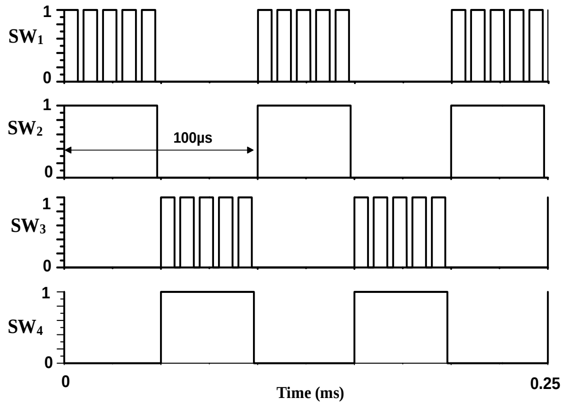

Fig. 3. The switching pulses at the gates of switches

When SW_1 is ON (or SW_3), energy is stored in the inductor "L_1" (or L_2) by the PV source. When SW_1 (or SW_3) is OFF, D_1 (or D_2) gets forward biased, discharging the inductor stored energy into capacitor C_{bi}, which continuously feeds current to the load. The switched gate signals for SW_1, SW_2, SW_3 and SW_4 are shown in Fig. 3.

B. Modified proposed topology

The target of the proposed topology is a 10 kHz square waveform output voltage that is linked to RIS by HFT. Therefore, the topology is designed to achieve many features of the complete system as mentioned previously. But at the instant of turning the operation between the two buck boost, the polarity of the capacitor voltage V_{Cbi} cannot change instantaneously. Although this time is very short, two paths of surge current appear due to high value of V_{Cbi} compared to the input voltage. Assuming the polarity of V_{Cbi} changed from the positive half cycle to negative half cycle and by referring to Fig. 2, the first path of surge current flows through capacitor C_{bi}, switch SW_4 and body diode of switch SW_2. The second path of surge current flows through capacitor C_{bi}, switch SW_4, input capacitor C_p and body diode of switch SW3. In order to limit this surge current, two stages of modification have been

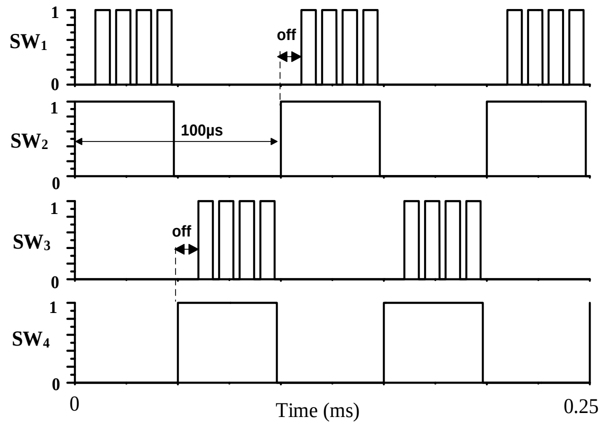

Fig. 4. The modified switching pulses at the gates of switches

proposed. The first one considers bi-directional switch for SW_2 and SW_4 and adding series diode in opposite direction of the body diode of SW_1 and SW_3. Consequently, the capacitor current I_{Cbi} is limited by flowing through inductor L_2. Although, the surge current is limited, it is added to the source current in inductor L_2 (SW_3 is ON) at the instant of changing the polarity of V_{Cbi}, resulting in rising the output voltage at the begging of each half cycle. In order to obtain proper square wave shape, the second stage of modification was done by keeping SW_1 and SW_3 in OFF state at this instant. The modified switched gate signals for SW_1 and SW_3 are shown in Fig. 4.

III. Operation Modes and Parameters Design

The operation modes of the boost inverter are similar for the basic version and the modified version of the proposed topology. The basic version topology has three modes of operation based on the switching of SW_1 during the positive half-cycle since the switch SW_2 is always ON during these three modes. In Mode1 as shown in Fig. 5, switch SW_1 is ON and energy is stored in the buck-boost inductor L_1 by the PV source. In Mode 2 as shown in Fig. 6, switch SW_1 is OFF and D_1 is forward biased, discharging the inductor stored energy into capacitor C_{bi}, which feeds current to the load (R). In Mode 3 as shown in Fig. 7, both SW_1 and D_1 are OFF as a result of DCM operation.

In mode 1 ($0 < t \leq T_{on}$) as shown in Fig. 5, inductor voltage and capacitor current in this mode are given as follows;

$$V_{L_1}(t) = L_1 \frac{dI_{L_1}(t)}{dt} = V_{pv}(t) \quad (1)$$

$$I_{c_{bi}}(t) = C_{bi} \frac{dV_{c_{bi}}(t)}{dt} = -\frac{V_o(t)}{R} \quad (2)$$

In mode 2 ($T_{on} < t \leq T_{off}$) as shown in Fig. 6, inductor voltage and capacitor current in this mode are given as follows;

$$V_{L_1}(t) = L_1 \frac{dI_{L_1}(t)}{dt} = -V_{c_{bi}}(t) = -V_o(t) \quad (3)$$

$$I_{c_{bi}}(t) = C_{bi} \frac{dV_{c_{bi}}(t)}{dt} = I_{L_1}(t) - \frac{V_o(t)}{R} \quad (4)$$

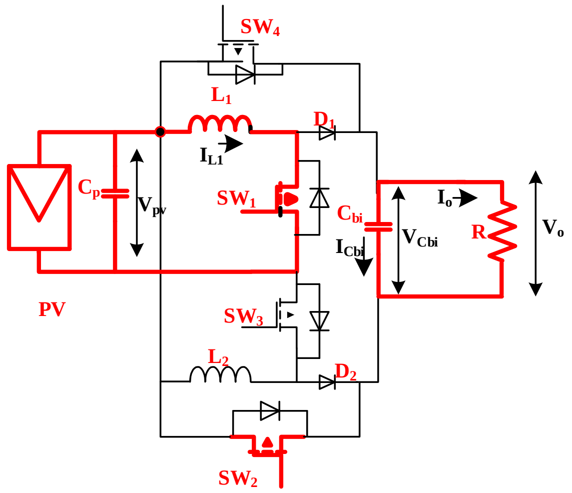

Fig. 5. Operation mode 1 when SW_1 is ON

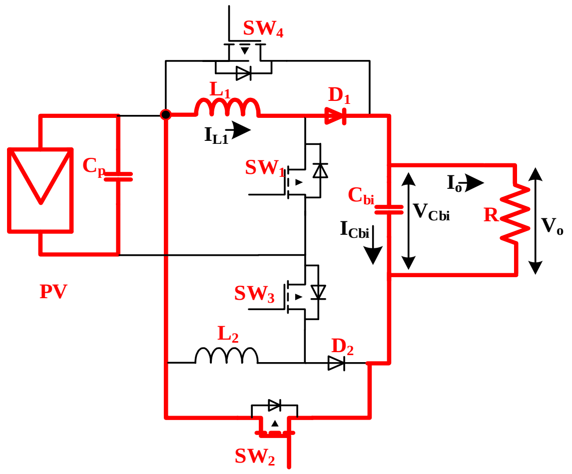

Fig. 6. Operation mode 2 when SW_1 is OFF and D_1 is ON

In mode 3 (Toff < t ≤ Td-off) as shown in Fig. 7, inductor voltage and capacitor current in this mode are given as follows;

$$V_{L_1}(t) = L_1 \frac{dI_{L_1}(t)}{dt} = 0 \quad (5)$$

$$I_{c_{bi}}(t) = C_{bi} \frac{dV_{c_{bi}}(t)}{dt} = -\frac{V_o(t)}{R} \quad (6)$$

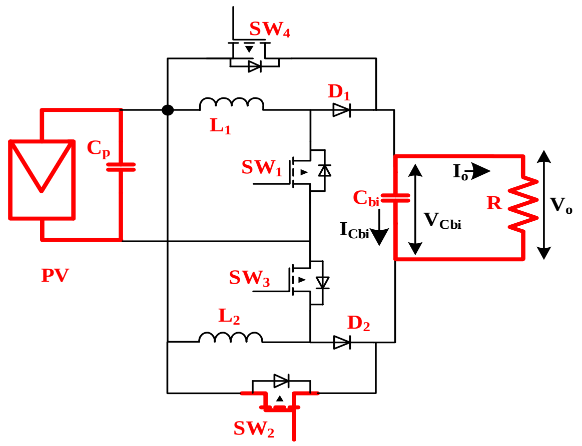

Fig. 7. Operation mode 3 when SW_1 and D_1 are OFF

Likewise, the inductor voltage and capacitor current can be obtained in the negative half-cycle of the high-frequency output voltage when the second buck-boost inverter is activated.

According to Mode 1, the energy drowns from the PV source is the following:

$$E_{pv}\ (t) = \frac{1}{2}\ L_1 I_{L_1}^2 \tag{7}$$

According to (1), the peak value of the inductor current can be formulated as follows;

$$\mathrm{I}_{\mathrm{L}_1} = \frac{\mathrm{V}_{\mathrm{pv}}}{L_1} D T_s \tag{8}$$

Substituting by (8) in (7) yields:

$$E_{pv}\ (t) = \frac{V_{pv}^2}{2L_1} D^2 {T_s}^2 \tag{9}$$

The energy transferred into the load during switching period T_s is given by:

$$\mathrm{E_o(t)} = \mathrm{V_o} \times I_o\ \times T_s = \frac{\mathrm{V_o}^2}{R} T_s \tag{10}$$

As a result of DCM operation, the stored energy in the buck-boost inductor L_1 (or L_2) is discharged into capacitor C_{bi}. then the capacitor C_{bi} feeds the stored energy into the load. Therefore, the energy delivered into the load $E_o(t)$ is equal to the energy drown from the source $E_{pv}(t)$ during the switching period T_s. Equalizing (9) and (10) yields the formula of the boost converter voltage gain as follows,

$$\frac{\mathrm{V_o}}{\mathrm{V_{pv}}} = \sqrt{\left(D^2 \times T_s \times \frac{R}{2L_1}\right)} \tag{11}$$

Equation (11) is used to determine the value of the inductor L_1, which results the following expression:

$$\mathrm{L}_1 \leq \frac{V_{pv}^2}{2P} D^2\ T_s \tag{12}$$

Where; P is the rated power transferred into the load, inductor L_2 has the same value as L_1.

According to [24], the value of capacitor C_{bi}, which is required to obtain a given output voltage ripple peak magnitude ΔV can be selected by the following expression:

$$\mathrm{C_{bi}} \leq \frac{L_1 I_{pk\_L1}^2}{4V_o\ \Delta V} \leq \frac{V_o T_S}{2R\ \Delta V} \tag{13}$$

Where; ΔV is the ripple of the capacitor voltage.

The second stage is the RIS, which consists of an H-bridge rectifier cascaded by an H-bridge inverter through DC-link capacitor C_{dc}. According to [25] C_{dc} is sized as follows;

$$C_{dc} = \frac{P_g}{2\omega V_{dc}\,\Delta V_{dc}} \tag{14}$$

Where; P_g is the average active power injected into the grid, ω is the line angular frequency in rad/sec and ΔV_{dc} is the amplitude of the DC-link voltage ripple.

IV. CONTROL STRATEGIES

The control of the proposed system is divided into two major strategies; PV side control and grid side control.

A. PV side control

The main challenge in using PV energy is its nonlinear current-voltage characteristics (I-V), which results in a unique MPP on the power-voltage (P-V) curve. Further complicating the matter is the dependence of these characteristics on solar insolation and temperature. Since these parameters are constantly changing, the MPP also varies. Considering the high initial capital cost of the PV source and its low energy conversion efficiency, it is necessary to operate the PV source at MPP so that the maximum power can be extracted. Therefore, the control strategy for the first stage of the proposed system fulfills two tasks. The first task is to extract the MPP of the PV source. In generally this control is called MPPT. Several MPPT techniques have been proposed in the last decades. P&O MPPT algorithm [٢6] is one of simple hill-climbing algorithms, which extensively used in practical PV systems because of its simplicity. Moreover, prior study or modeling of PV characteristics is not required. The second task is to operate the HFBI switches in such a way that they give a square wave voltage of 10 kHz.

Although the implementation of the P&O algorithm is simple, it has some drawbacks such as the oscillation of the operating point around the MPP at steady state, which raises the waste of some amount of available energy. In addition, the P&O algorithm can be confused by rapidly changing atmospheric conditions. In some literatures [27-28], the negative effects of the P&O algorithm drawbacks are limited. The flow chart of P&O MPPT algorithm is depicted on Fig. 8. When the perturbation of the algorithm has three-level at steady state, it indicates the algorithm is stable and swings around the MPP. The perturbation of the algorithm is compared with 100 kHz saw-tooth carrier signal and the resulting pulses are used to drive HFBI switches.

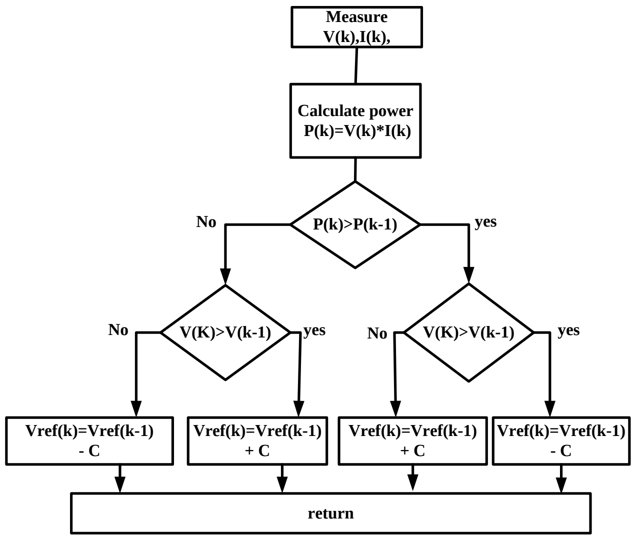

Fig. 8. Flowchart of the P&O algorithm

B. Grid side control

The grid side control is assigned with many tasks such as control of the active power injected to the grid, grid synchronization, inject sinusoidal current to the grid with minimum THD and unity power factor, in addition to DC-link voltage control.

1) Grid synchronization

For unity power factor control, the inverter output current must be synchronized with the grid voltage. The synchronization is achieved by using the phase angle of the grid voltage to convert the feedback variables into a suitable reference frame. phase-locked loop (PLL) is one of the most common synchronization techniques for extracting the phase angle of the grid voltages.

2) Current control

Current control is more efficient than voltage control for controlling three-phase grid inverter [29]. Current controller has fast response and less sensitive to distortion in grid voltage. Linear proportional-integral (PI) controller is widely used in current control, it provides proper response low harmonic content, constant switching frequency. PI controller calculates the error between a sensed inverter output current and a desired injected current to the grid and then the controller minimizes this error. In synchronous (dq) reference frame, the control variables become DC and the PI compensators are able to reduce the error to zero.

The synchronous controller block diagram for the grid connected inverter is shown in Fig. 1. The inner control loops have two PI controllers to compensate the dq current components. PI compensators reduce the error(s) between the desired current I_d* (I_q*) and the actual current I_d (I_q) to zero. The output energy and power factor can be controlled via changing d-axis current and q-axis current. For improving the performance of PI controller in such a structure, cross-coupling terms and voltage feed forward are usually used [30].

2) Dc-link voltage control

For proper operation of the grid connected inverter, the input DC voltage to the inverter is kept at steady voltage level. Therefore, the outer control loop has PI controller to stabilize the DC-voltage link to the reference voltage.

V. SIMULATION RESULTS

In order to validate the operation of the proposed system, it has been carried out in PSIM software (ver. 10.0). 5 kW PV array is simulated at 25° C temperature and 1000 W/m^2 radiation. The simulated circuit parameters and the electrical characteristics of PV array at MPP are listed in Table 1. Switches SW_1 and SW_3 are responsible of boosting the input voltage. Therefore, they switched by 100 kHz and their duty cycles are modulated by MPPT algorithm. Switches SW_2 and SW_4 are responsible of inverting process; hence they are switched by 10 kHz 0.5 duty cycle. Switches of H bridge inverter in the grid side are modulated by the synchronous controller to inject a sinusoidal current into the grid and in-phase with the grid voltage for unity power factor.

TABLE I. PROPOSED SIMULATED CIRCUIT PARAMETERS

Symbol	Meaning	Value
$L_1=L_2$	HFBI inductors	17.5 µH
C_{bi}	HFBI capacitor	330 nF
C_d	Dc link capacitor	1٠٠0 µf
L_g	grid filter inductor	3 mH
V_{pv} I_{pv} P_{pv}	Electrical characteristics of PV module at MPP.	180 V 28 A 5 kW

Fig. 9 shows the PV outputs (V_{PV}, I_{PV} and P_{PV}) at MPP and the duty cycle perturbation (output of MPPT algorithm). It is clear that the duty cycle perturbation has three-level at steady state, which indicates that P&O MPPT algorithm is stable and swings around the MPP.

Fig. 10 shows the three-phase grid currents at steady-state MPPT algorithm. It is clear from the figure; the injected grid current is in-phase with the grid voltage. The figure also shows the DC-link voltage, which controlled with 400V reference value. The frequency of the primary voltage V_{Cbi} of HFT is high frequency, as shown in Fig. 10, which is the output of the proposed topology HFBI therefore, Fig. 10 is magnified to show this waveform and other high frequency signal waveforms of HFBI in suitable view, as shown in Fig. 11. Switches gate signals V_{g1}, and V_{g3} are 100 kHz and Switches gate signals V_{g2}, and V_{g4} are 10 kHz 0.5 duty cycle. The boost inverter capacitor voltage V_{Cbi} is square wave at 10 kHz. The inductor current I_{L1} is DCM to avoid the circulating current between the inductor and the parallel-connected switch in the next operating half cycle.

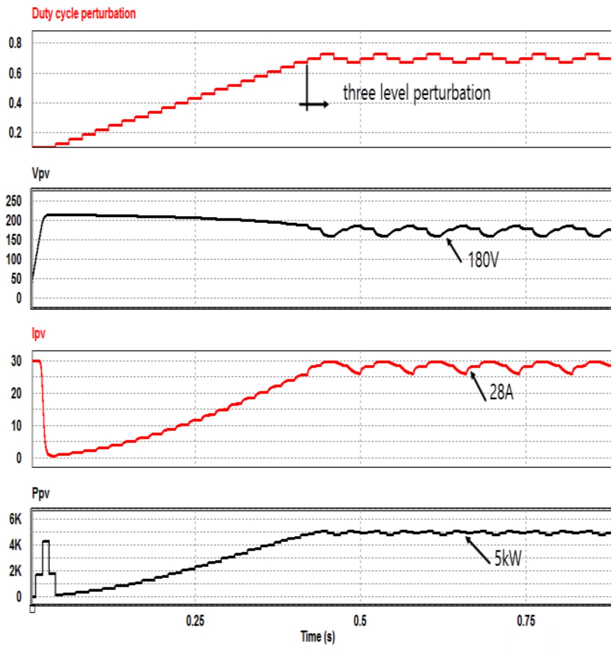

Fig. 9. I_{pv}, V_{pv} and P_{pv} of PV array at MPP and the duty cycle perturbation

VI. CONCLUSION

This paper has proposed a new single-stage high-frequency boost inverter cascaded by Rectifier-inverter system for PV grid-tie applications. The topology has been analyzed, designed and simulated. The topology performs many features such as MPPT, boosting PV voltage in addition to the high frequency square wave output voltage that allows the use of HFT to guarantee galvanic isolation between the grid and the PV system, in addition to overcoming the drawbacks of conventional line frequency transformer. The proposed HFBI topology is one stage with reduced power switches compared with the conventional topologies.

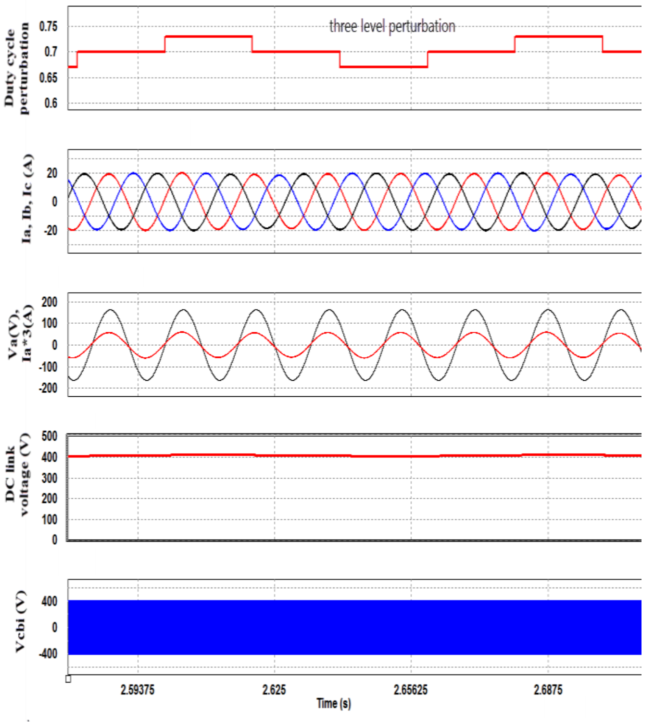

Fig. 10. Three-phase grid currents, DC-link voltage, and HFBI capacitor voltage V_{Cbi}

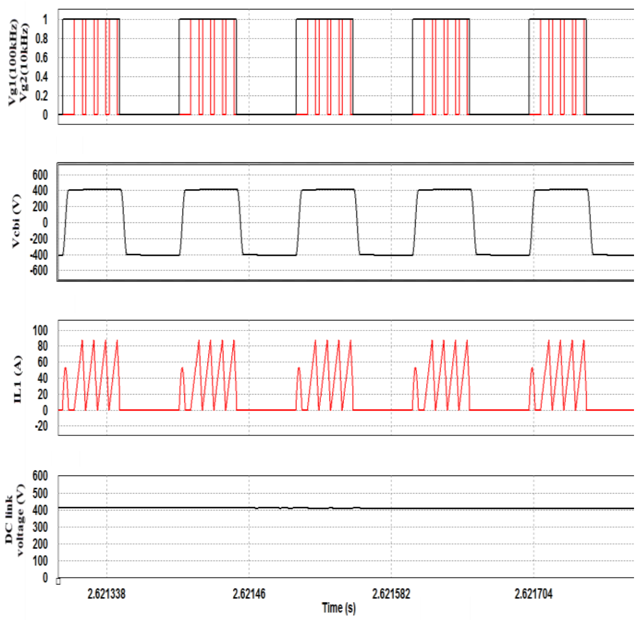

Fig. 11. HFBI switches gate signals, V_{Cbi}, inductor current, and DC-link voltage

The presented simulated results demonstrate a boosting of PV array voltage; therefore low PV array voltages can be stepped up to levels commensurate with the grid voltage. Consequently, the use of a few series connected solar panels is sufficient. This avoids environmental changes such as shadow, which reduces the utilization of solar panels. Simulation results, which emphasizing the performance of the proposed topology of proposed system, have been validated.

REFERENCES

[1] F. Blaabjerg, F. Iov, T. Kerekes, and R. Teodorescu, "Trends in power electronics and control of renewable energy systems", 14th Int. Power Electronics and Motion Control Conf. (EPE/PEMC) 1, K-1–K-19 (2010).

[2] EPIA, "Global market outlook for photovoltaics until 2013", Eur. Photovoltaic Industry Association 1, CD-ROM (2010).

[3] Chetan Singh Solanki "Solar Photovoltaics: Fundamental, Technology and application" Second Edition-2011, Book Published by: PHI Learning Private Ltd., New Delhi

[4] G. Petrone, G. Spagnuolo, R. Teodorescu, M. Veerachary, and M. Vitelli, "Reliability issues in photovoltaic power processing systems," IEEE Trans. Ind. Electron., vol. 55, no. 7, pp. 2569–2580, Jul. 2008.

[5] R. H. Wills, S. Krauthamer, A. Bulawka, and J. P. Posbic, "The AC photovoltaic module concept," in Proc. 32nd IECEC, 1997, vol. 3, pp. 1562–1563.

[6] Y. Chen and K. M. Smedley, "A cost-effective single-stage inverter with maximum power point tracking," IEEE Trans. Power Electron., vol. 19, no. 5, pp. 1289–1294, Sep. 2004.

[7] S. Jain and V. Agarwal, "A single-stage grid connected inverter topology for solar PV systems with maximum power point tracking," IEEE Trans. Power Electron., vol. 22, no. 5, pp. 1928–1940, Sep. 2007.

[8] D. C. Martins and R. Demonti, "Grid connected PV system using two energy processing stages," in Conf. Rec. 29th IEEE Photovoltaic. Spec. Conf., 2002, pp. 1649–1652.

[9] L. Zhang, K. Sun, L. Feng, H. Wu, and Y. Xing, "A family of neutral point clamped full-bridge topologies for transformerless photovoltaic grid-tied inverters," IEEE Trans. Power Electron., vol. 28, no. 2, pp. 730–739, Feb. 2013.

[10] B. N. Alajmi, K. H. Ahmed, G. P. Adam, and B. W. Williams, "Single phase single-stage transformerless grid-connected PV system," IEEE Trans. Power Electron., vol. 28, no. 6, pp. 2664–2676, Jun. 2013.

[11] S. V. Araujo, P. Zacharias, and R. Mallwitz, "Highly efficient single phase transformerless inverters for grid-connected photovoltaic systems," IEEE Trans. Ind. Electron., vol. 57, no. 9, pp. 3118–3128, Sep. 2010.

[12] T. Kerekes, R. Teodorescu, M. Liserre, C. Klumpner, and M. Sumner, "Evaluation of three-phase transformerless photovoltaic inverter topologies," IEEE Trans. Power Electron., vol. 24, no. 9, pp. 2202–2211, Sep. 2009.

[13] D. Meneses, F. Blaabjerg, O. Garc´ıa, and J. A. Cobos, "Review and comparison of step-up transformerless topologies for photovoltaic ac-module application," IEEE Trans. Power Electron., vol. 28, no. 6, pp. 2649–2663, Jun. 2013.

[14] M. Calais and V. G. Agelidis, "Multilevel converters for single-phase grid connected photovoltaic systems-an overview," in Proc. IEEE Int. Symp. Ind. Electron., 1998, pp. 224–229.

[15] V. Meksarik, S. Masri, S. Taib, and C. M. Hadzer, "Development of high efficiency boost converter for photovoltaic application," in Proc. National Power Energy Conf., 2004, pp. 153–157.

[16] B. M. T. Ho and H. S. Chung, "An integrated inverter with maximum power tracking for grid-connected PV systems," IEEE Trans. Power Electron., vol. 20, no. 4, pp. 953–962, Jul. 2005.

[17] S. B. Kjær, J. K. Pedersen, and F. Blaabjerg, "Power inverter topologies for photovoltaic modules—A review," in Proc. IEEE IAS, 2002, pp. 782–788.

[18] S. B. Kjær, J. K. Pedersen, and F. Blaabjerg, “A review of single-phase grid-connected inverters for photovoltaic modules,” IEEE Trans. Ind. Appl., vol. 41, no. 5, pp. 1292–1306, Sep./Oct. 2005.

[19] X. Li and A. K. S. Bhat, “A utility-interfaced phase-modulated high frequency isolated dual LCL DC/AC converter,” IEEE Trans. Ind. Electron., vol. 59, no. 2, pp. 1008-1019, Feb. 2012.

[20] H. Qin and J. W. Kimball, “Closed-loop control of DC–DC dual-active bridge converters driving single-phase inverters,” IEEE Trans. Power Electron., vol. 29, no. 2, pp. 1006-1017, Feb. 2014.

[21] H. Qin and J. W. Kimball, “Closed-loop control of DC–DC dual-active bridge converters driving single-phase inverters,” IEEE Trans. Power Electron., vol. 29, no. 2, pp. 1006-1017, Feb. 2014.

[22] L. Quan and P. Wolfs, “A Review of the Single Phase Photovoltaic Module Integrated Converter Topologies With Three Different DC Link Configurations,” IEEE Trans. Power Electron., vol. 23, no. 3, pp. 1320 - 1333, 2008.

[23] M. A. Sayed, K. Suzuki, T. Takesita, W. Kitagawa, “Soft-Switching PWM Technique for Grid-Tie Isolated Bidirectional DC-AC Converter With SiC Device,” IEEE Trans. Industry Applications, vol. 53, no. 6, pp. 5602–5614, 2017.

[24] M. A. Sayed, K. Suzuki, T. Takesita, W. Kitagawa, “PWM Switching Technique for Three-Phase Bidirectional Grid-Tie DC-AC-AC Converter with High-Frequency Isolated,” IEEE Trans. Power Electron., vol. 3, no. 1, pp. 845–858, 2018.

[25] S. B. Kjaer, J. K. Pedersen, and F. Blaabjerg, “A review of single-phase grid-connected inverters for photovoltaic modules,” IEEE Transactions on Industry Applications, vol. 41, no. 5. pp. 1292–1306, 2005.

[26] C. Hua, J. Lin, C. Shen, “Implementation of a DSP-controlled photovoltaic system with peak power tracking,” IEEE Trans. Ind. Electron. 45 (1) (1998) 99‑107.

[27] N. Femia, G. Petrone, G. Spagnuolo, and M. Vitelli. “Optimization of perturb and observe maximum power point tracking method,” IEEE Transactions on Power Electronics, 20(4):963–973, 2005.

[28] H. Radwan , Mahmoud A. Sayed ,Adel A. Elbaset and G. Shabib , “The Non Ideality Effect of Optimizing the P&O MPPT Algorithm for PV AC Load Applications ”, 17th International MiddleEast Power System Conference (MEPCON'15) Mansoura University, Egypt, December 15-17, 2015.

[29] Sung-Hun Ko, Seong R. Lee, Hooman Dehbonei, Chemmangot V. Nayar. “Application of Voltage- and Current-Controlled Voltage Source Inverters for Distributed Generation Systems,” s.l. : IEEE Transactions On Energy Conversion, September 2006. pp. VOL. 21, NO. 3.

[30] Frede Blaabjerg, Remus Teodorescu, Marco Liserre, Adrian V. Timbus. “Overview of Control and Grid Synchronization for Distributed Power Generation Systems,” s.l. : IEEE Transactions On Industrial Electronics, October 2006. pp. VOL. 53, NO. 5.